Article

High-throughput virtual screening of novel rilpivirine analogs as next-generation antiretroviral therapeutics

Jeslyn Wu[1,2], Charissa Luk[1,3], Catherine Zhou[1,4], Aashi Shah[1,5], Aishwarya Yuvaraj[1,6], Edward Njoo[1]

[1] Aspiring Scholars Directed Research Program, Fremont, CA

[2] Mission San Jose High School, Fremont, CA

[3] Bishop O'Dowd High School, Oakland, CA

[4] Lynbrook High School, San Jose, CA

[5] Amador Valley High School, Pleasanton, CA

[6] American High School, Fremont, CA

SUMMARY

Part of the retroviral genus, the human immunodeficiency virus (HIV) relies on the host's cellular machinery for replication. The viral genetic material is composed of ribonucleic acid (RNA) which, upon delivery into the host's cells, is reverse transcribed into deoxyribonucleic acid (DNA) by the viral enzyme reverse transcriptase (RT). This is then used for the production of new viral components, thus allowing for further replication and spread of HIV. Because this virus selectively targets CD4+ T cells, the infection inevitably leads to weakening of the host's immune system, which can then lead to acquired immunodeficiency syndrome (AIDS). One treatment for HIV is non-nucleoside reverse transcriptase inhibitors (NNRTIs), which are allosteric inhibitors of RT that disable the enzyme's activity and thus viral replication. Previous NNRTIs approved for clinical use by the United States Food and Drug Association (FDA) include etravirine, doravirine, and rilpivirine. However, resistance to these drugs through mutations in RT necessitates the continued development of NNRTIs. Here, the structure of rilpivirine, a relatively recently FDA approved NNRTI, was used to design a library of analogs that were then evaluated in silico via high-throughput virtual screening (HTVS). From this, several structures were identified as potential next-generation NNRTIs with comparable predicted binding affinities to the allosteric binding pocket in RT as rilpivirine.

INTRODUCTION

As of 2019, approximately 38 million people across the globe have human immunodeficiency virus/acquired immunodeficiency syndrome (HIV/AIDS) (1). Without any treatment, the retrovirus can replicate billions of times a day to quickly weaken the immune system of the host and eventually cause AIDS. The virus weakens a system by selective targeting the CD4+ T cells of the host. A person is considered to have progressed to AIDS when their CD4+ T cell count is lower than 200 cells per cubic millimeter of blood (cells/mm^3). For reference, the CD4+ T cell count ranges from 500 to 1,600 cells/mm^3 in a person with a healthy immune system. This loss of the host's CD4+ T helper cells results in the destruction and functional impairment of the immune system. HIV/AIDS often prove fatal for patients because opportunistic illnesses (OIs) and cancers that are usually controlled in immunocompetent people can become serious fatal threats to those with a weakened immune system. Enabling accessible HIV treatment for all is the key to ending AIDS as a public health threat as well as the only viable way infected individuals can live longer and healthier lives (2).

Current treatments are called antiretroviral therapy (ART), combination therapy, and highly active antiretroviral therapy (HAART) because of the utilization of at least two HIV drugs meant to treat the infection (3). With treatment, people are able to live normally and avoid AIDS. One class of drugs used is non-nucleoside reverse transcriptase inhibitors (NNRTIs), which are allosteric inhibitors of the reverse transcriptase (RT) enzyme in HIV. The process of viral replication and spread relies on the transformation of viral RNA into DNA that then allows viral reproduction within host cells. The RT enzyme is vital to the viral reproduction system. As allosteric inhibitors, NNRTIs effectively block the enzyme from converting viral RNA into DNA by binding at a region of RT that configures the enzyme to perform worse. In RT, this then prevents HIV from further replication (4).

The first generation NNRTIs are nevirapine, delavirdine, and efavirenz (5, 6, 7) (**Figure 1**). This generation proved to have decent efficacy relative to preceding treatments; however, errors like delavirdine's ineffectiveness on its own proved to be setbacks as it required the usage of multiple drugs combined. These compounds all have a low genetic barrier to resistance, meaning a single mutation in the RT sequence can lead to effective drug resistance (8, 9). Consequently, the second generation of NNRTIs, etravirine and rilpivirine, were designed to better combat RT mutations. Compared to the first generation of NNRTIs, these drugs showed stronger inhibitory activity, especially against the HIV mutations that caused first generation NNRTIs to be less successful (10). Additionally, doravirine, a part of the newest generation, has also been recently FDA approved (11, 12).

Currently, only the six aforementioned NNRTIs shown in **Figure 1** (nevirapine, delavirdine, efavirenz, etravirine, rilpivirine, and doravirine) have been approved by the FDA. The development of these drugs has evolved greatly over the past 30 years and further investigation into synthesis will be essential to the discovery of the next generation of cost-effective NNRTIs (13).

The rapid drug-resistant mutations in HIV-1 RT, dose-limiting toxicity, and unfavorable pharmacokinetic properties
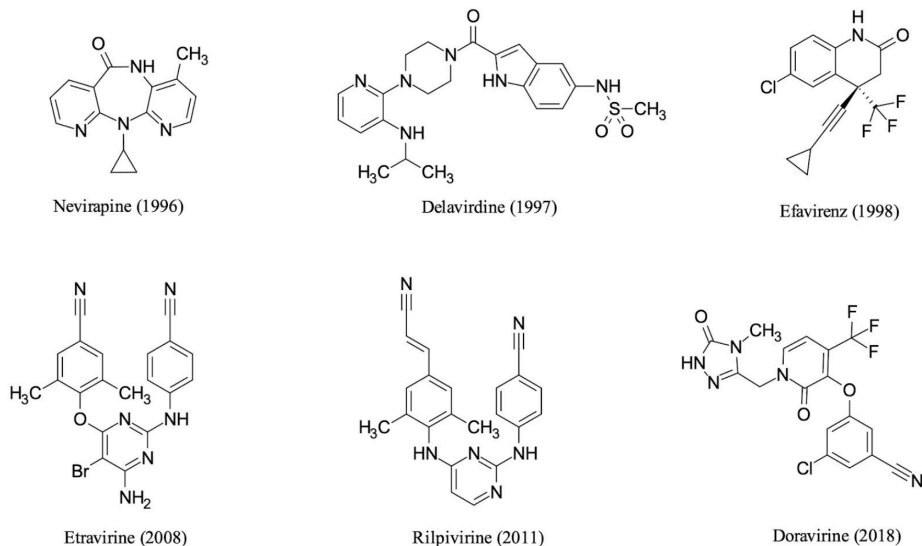
Figure 1: Chemical structures of FDA-approved NNRTIs. The six NNRTIs currently approved by the FDA are nevirapine, delavirdine, efavirenz, etravirine, rilpivirine, and doravirine.

should be considered and avoided for effective anti-HIV therapy. In order to account for these problems, structural mimics of a range of scaffolds or peripheral substituents are possibilities of promising inhibitors for HIV-1 RT; however, these methods are still not fully effective. Structure-based bioisosterism was also previously attempted in NNRTI development (14). Such NNRTIs include piperidine-substituted thiophene[2,3-d]pyrimidine derivatives, which were shown to have high resistance profiles, improved solubilities, lower cytochrome liabilities, and human ether-a-go-go gene inhibition, making them potent inhibitors in the MT-4 cells line (15). These studies determined that the effective properties mainly include structural flexibility and numerous hydrophobic interactions to form a H-bond (hydrogen bond) network with the NNRTI binding pocket. Overall, these properties account for increased activity against cross resistance-associated mutations.

Specifically, rilpivirine, a second-generation NNRTI, has higher potency, a longer half-life, and relatively fewer side effects compared to other NNRTIs. Rilpivirine is a diaryl pyrimidine (DAPY) compound with a butterfly conformation (16). DAPY analogues, with a characteristic "horseshoe" or

"U-shape" structure, have been studied extensively over the past two decades for their high potency and relatively low cytotoxicity (17). Furthermore, they are active against wild-type viruses and retain activity against previous NNRTI-resistant HIV-1 strains *in vitro*. The internal conformational flexibility of rilpivirine as well as the plasticity of the interaction between rilpivirine and the NNRTI-binding site of HIV RT allows the compound to bind in different modes, giving it greater tolerance to binding pocket mutations in RT (18), which contains lysine, phenylalanine, tryptophan, and tyrosine. The tryptophan, phenylalanine, and tyrosine residues in the NNRTI binding pocket are able to form aromatic-aromatic interactions that are no more than 7 Å in distance with an inter-plane angle between 30° to 90° (19). Three types of interactions can be found with aromatic systems: π-π, cation-π, and X-H-π, where X is carbon, oxygen, nitrogen, boron, or a halogen like fluorine, chlorine, or bromine. There are four general types of aromatic π-π interaction geometries: face-to-face (sandwich), parallel-displacement, T-shaped, and edge-to-face; however, face-to-face is not favorable and thus is rarely observed. Lysine and arginine are generally able to form polar cationic-π interactions within 6 Å.
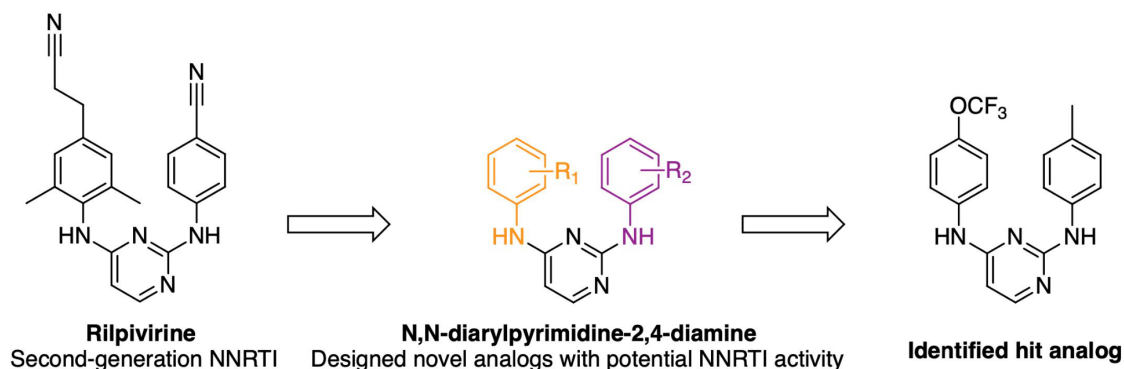

Figure 2: Design and core scaffold of the library of our structural analogs of rilpivirine. Starting from rilpivirine (left), the base structure of all analogs is created. Screening then identifies analogs with the best activity, one of which is drawn (right).

Modern advances in computational modeling have allowed for high-throughput virtual screening (HTVS) of vast compound libraries much more rapidly than can be synthesized and evaluated for potential biological activity in a laboratory. We proposed that this approach could be used to develop structural analogs to rilpivirine as potential next-generation NNRTIs. Here, we report the *in silico* design and HTVS of a library of 196 N,N-diarylpyrimidine-2,4-diamines as structural analogs of rilpivirine, which could conceivably be synthesized from a library of fragments and 2,4-dichloropyrimidine (**Figure 2**). Moreover, identified top analogs allowed us to hypothesize that analogs with better electron-withdrawing functionalities at the substituted positions (R1 and R2 in **Figure** 2) would return the highest predicted binding affinities due to their structural similarity to rilpivirine.

RESULTS

Substitutions at the 2 and 4 positions of the designed base analog allowed for 196 rilpivirine analogs to be computationally screened in a HTVS to simulate biological activity (**Figure 3**). Fragments chosen for the substitutions included various varieties differing in their electron withdrawing capabilities to potentially lead towards a conclusion on the most effective. Compounds 4G, 7D, 10D, 4E, and 7B produced the most favorable binding affinities. Compared to rilpivirine, which returned a predicted binding affinity of -12.7 kcal/mol by the same docking parameters, compounds with comparable and even better binding affinities were identified (**Figure 4**). These

compounds further advance the research done on developing novel NNRTIs.

3MEE

The docking of our rilpivirine analogs to HIV-1 reverse transcriptase [PDB: 3MEE] (20) indicate that 4G, 7D, 10D, 4E, and 7B (12.8, 12.5, 12.5, 12.4, and 12.4 kcal/mol, respectively) have the highest binding affinities. These analogs bound with the known NNRTI binding pocket are visualized in **Figure 4** using Chimera (21).

4G: 4-trifluoromethoxy aniline fragment as R1 and 4-amino toluene fragment as R2

The binding affinity of rilpivirine to 3MEE is -12.7 kcal/mol, and 4G has a greater binding affinity of -12.8 kcal/mol. The methyl end of the R1 group, 4-amino toluene, forms a hydrophobic interaction with the aromatic ring of phenylalanine 227 at a distance of 4.30 Å. Glutamic acid 138 and lysine 103 are able to form relatively weak H-bond interactions with NH on R2 and R1 at distances of 4.39 Å and 3.84 Å, respectively. The trifluoromethoxy end of the R2 group, 4-trifluoromethoxy aniline, forms a halogen-π interaction with tyrosine 188 at a distance of 3.5 Å, and another halogen-π interaction with tryptophan 229 at a distance of 4.1 Å. The fluorine also forms an OH-F interaction, where OH, the hydroxyl end of tyrosine 188, is 3.75 Å away. The ring of the 4-trifluoromethoxy aniline fragment forms a π-π interaction with the aromatic ring of tyrosine 181 at a measured distance of 4.3 Å. Overall, these

R2 \ R1	Structure	1	2	3	4	5	6	7	8	9	10	11	12	13	14
A		-10	-11	-10.6	-11.2	-10.9	-10.5	-10.7	-10.4	-9.4	-10	-10.1	-4.8	-7.6	-4.8
B		-11.2	-10.5	-11.5	-11.9	-11.6	-9.6	-12.4	-10.4	-10.6	-11.8	-11.2	-7.2	-10.3	-8.9
C		-11.1	-11.6	-9.9	-11.7	-10.8	-11	-11.1	-11	-10.8	-10.3	-11.1	-9	-9.2	-7.9
D		-11.7	-11.5	-11.8	-11.5	-12.1	-11.6	-12.5	-11	-11.3	-12.5	-7.5	-4.1	-12	-7.9
E		-10.3	-11.6	-10.5	-12.4	-9.6	-10.4	-11.9	-10.6	-10.9	-10.8	-11.1	-8.3	-9.2	-8.1
F		-11.3	-10.9	-9.7	-11.6	-9.9	-9.9	-11.2	-10.9	-10.5	-10.3	-10.8	-9	-8.8	-7.8
G		-12	-12	-11.6	-12.8	-11.6	-11.3	-12.3	-10.9	-11.3	-11.9	-11.3	-10.8	-10.9	-9
H		-10.5	-10.2	-10.6	-10.9	-10.5	-10.8	-10.8	-10	-10.2	-10.6	-10.4	-10	-10	-9.8
I		-10.3	-10.4	-10.6	-11.2	-10.8	-10.4	-11.1	-10.1	-10.3	-10.9	-10.5	-9.9	-9.6	-9.4
J		-11.2	-11.3	-10.3	-10.3	-10.2	-10.2	-10.5	-10.7	-11	-10.4	-11.1	-9.1	-9	-8.4
K		-11	-10.9	-10.5	-11.5	-10.8	-9.7	-11.1	-10.3	-10.7	-10.9	-10.6	-8.7	-9.5	-8
L		-9.4	-9.6	-8.8	-9.7	-8.5	-8.6	-10.6	-9.9	-9.7	-8.9	-9.4	-7.4	-5.7	-5.4
M		-9.7	-9.9	-8.9	-10.4	-8.5	-8.6	-10.6	-10.1	-9.4	-9	-9.2	-5.9	-9.4	-5.6
N		-9	-9.5	-7.2	-8.3	-8.3	-8.1	-9.1	-9.8	-8.9	-7.5	-8.4	-5	-5.2	-5.5

Docking Key	≤ -12	-11.99 to -11	-10.99 to -10	-9.99 to -9	-8.99 to -8	≥ -7.99

Figure 3: Computational screening results as a table. Heat map of structure-activity relationship (SAR) of predicted binding affinities in kcal/mol generated from molecular docking simulations of targeted rilpivirine analogs to reverse transcriptase (PDB:3MEE). Lower binding affinities signify higher biological activity. Calculated binding affinities are reported in kcal/mol for each aryl substitution pattern (R1, x-axis; R2; y-axis) on the core analog scaffold and are color coded according to the key shown. Under the same docking parameters, rilpivirine returned a binding affinity of -12.7 kcal/mol.
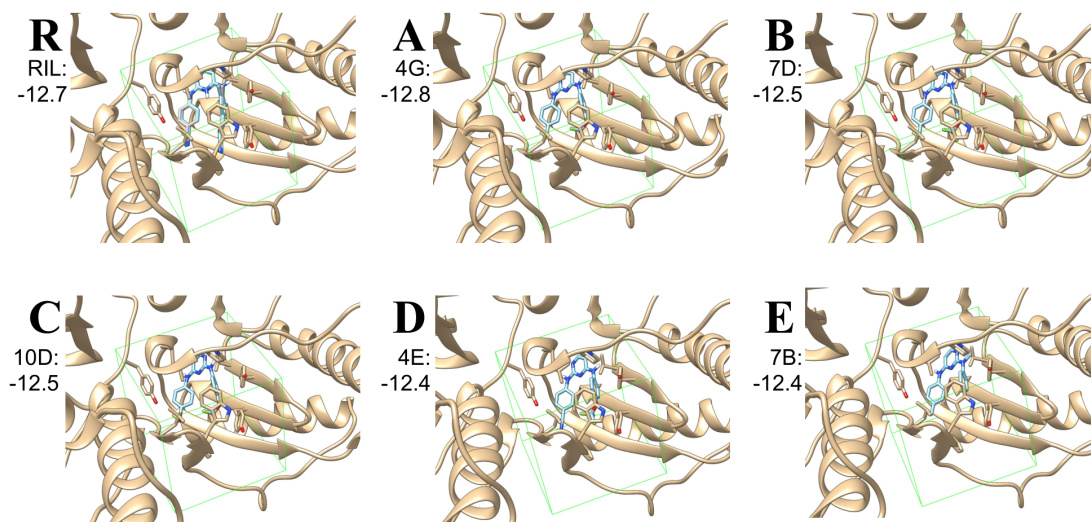
Figure 4: Identified hit analogs. The top five docked analogs as compared to rilpivirine docked to the same PDB with the same parameters. The shown analogs are labeled as follows: R: Rilpivirine layered with the original PDB, A: 4G. B: 7D, C: 10D, D: 4E, E: 7B.

extensive aromatic and hydrophobic interactions contribute to the high binding affinity of 4G.

7D: 4-amino toluene fragment as R1 and 4-trifluoro-methoxy aniline fragment as R2

The methyl end of the R1 group, 4-amino toluene, interacts in a hydrophobic interaction with the aromatic ring of phenylalanine 227 with a distance of 4.25 Å. Again, the R1 and R2 NH form weak electrophilic hydrogen interactions with glutamic acid 138 and lysine 103 at distances of 4.60 Å and 3.95 Å, respectively. These distances are farther than those seen in 4G, which has the same fragments in opposite positions but a higher binding affinity; therefore, this decrease in H-bonds is a probable cause for 7D's lower binding affinity compared to 4G. Additionally, a π-π interaction occurs between the R2 group, 4-trifluoromethoxy aniline, and tyrosine 183 at a distance of 4.3 Å. The trifluoro end forms the same interactions as those in 4G at relatively similar distances. Likewise, aromatic and hydrophobic interactions improve binding score like in 4G; however, weaker H-bonds contribute to 7D's relatively lower binding affinity compared to 4G.

10D: 4-bromoaniline fragment as R1 and 4-trifluoro-methoxy aniline fragment as R2

The brominated end of the R1 group, 4-bromoaniline, forms a halogen-π interaction with the aromatic phenylalanine 227, with a distance of 4.01 Å. The bromine also forms a halogen-hydroxyl interaction with the OH end of tyrosine 318 at a distance of 4.43 Å. Glutamic acid 138 and lysine 103 are able to form relatively weak H-bond interactions with NH on R1 and R2 at distances of 4.34 Å and 3.79 Å, respectively. The trifluoromethoxy end of the R1 group, 4-trifluoromethoxy aniline, forms one halogen-π interaction with tyrosine 188 at a distance of 3.6 Å and another halogen-π interaction with tryptophan 229 at a distance of 4.0 Å. The fluorine also forms an OH-X (where X is a halogen, in this case fluorine) interaction, where OH, the hydroxyl end of tyrosine 188 is 3.72 Å away. The ring of 4-trifluoromethoxy aniline forms a π-π interaction with the aromatic ring of tyrosine 181 at a distance

of 4.3 Å. Overall, 10D has two halogenated fragments, which contributes to its high binding affinity. Despite these two fragments, weaker interactions likely caused a lower score as compared to the previous two identified analogs.

4E: 4-amino benzonitrile fragment as R1 and 4-trifluoro-methoxy aniline fragment as R2

The R1 group, 4-aminobenzonitrile, interacts with phenylalanine 227 in the phenylalanine-proline part of the binding pocket 3.54 Å away. The 4-aminobenzonitrile ring forms a π-π interaction with the aromatic ring of tyrosine 318 at an angle of 48.8° and a distance of 5.1 Å. Glutamic acid 138 is able to form a relatively weak H-bond interaction with NH on R2 at a distance of 4.92 Å. The trifluoromethoxy end of the R2 group, 4-trifluoromethoxy aniline, forms a halogen-π interaction with tyrosine 188, at a distance of 3.5 Å, and another halogen-π interaction with tryptophan 229 at a distance of 4.2 Å. The fluorine also forms an OH-X (where X is a halogen, in this case fluorine) interaction, where OH, the hydroxyl end of tyrosine 188, is 3.72 Å away. The ring of 4-trifluoromethoxy aniline forms a π-π interaction with the aromatic ring of tyrosine 181 at a distance of 4.3 Å and an angle of 30.0°. 4E contains a fluorinated group which contributes to its high binding affinity and also a benzonitrile similar to that found in rilpivirine. Similar to 4E, weaker interactions likely caused a lower score.

7B: 4-amino toluene fragment as R1 and N-methylaniline fragment as R2

The R2 group N-methylaniline and aromatic tyrosine 181 forms a π-π interaction 4.3 Å away and at a 18.9° angle. The NH on R2 is able to form a NH-OH bond with the OH on glutamic acid 138 at a distance of 4.78 Å. The NH on R1 is able to form a relatively weak H-bond interaction with lysine 103 at a distance of 4.27 Å. The ring on R1, 4-amino toluene, forms a π-π interaction with the aromatic ring on tyrosine 318 at a distance of 5.5 Å and a dihedral angle of 45.8°.

DISCUSSION

Of the 196 rilpivirine analogs that were computationally

screened, we observed that analogs with a trifluoromethoxy group had a higher predicted binding affinity. This is in line with our original hypothesis relating higher binding affinities with better electron-withdrawing fragments. This activity can be rationalized with its high electron density and polarizability of the trifluoromethoxy fragment as well as fluorine's high electronegativity, high stability of the C-F bond in comparison to a C-H bond, and high lipophilicity. Additionally, trifluoromethoxy forms a halogen-π interaction with nearby tryptophan 229 and tyrosine 188, therefore improving binding affinity. This trend is supported by previous literature showing that the activity of other small molecule targets benefits from the addition of a halogen in the molecule (22). In this case, the fluorination of our analogs proved beneficial. The aniline ring also forms an aromatic π-stacking interaction with the aromatic amino acid tyrosine 181. The relatively low electron density pyrimidine ring forms strong electrostatic and H-bond interactions with glutamic acid 138 and lysine 103, both of which are charged residues at physiological pH. The methyl end of the ligand can also form CH-π interactions with aromatic phenylalanine 227. The docked position of each rilpivirine analog in the same allosteric binding site is visually shown (**Figure 4**).

Mutations in RT can arise from prolonged usage of NNRTIs. Thus, it is crucial to create analogs with improved potency against HIV-1 wild type and NNRTI-resistant strains. We plan to further study the binding affinity of our analogs compared to rilpivirine against clinically relevant mutant strains that confer NNRTI resistance, such as K101N, E138K, V179L, Y181C, Y188L and common double and triple mutants L100I/K103N, L100I/K103R/V179D, K103N/Y181C, V106A/Y181C through homology modeling (23).

This study's screening of analogs shows promising analogs for future NNRTIs compared to current NNRTIs, especially rilpivirine. The five top analogs from the docked library show similar trends in which attached R groups perform best. Either 4-trifluoromethoxy aniline and 4-amino toluene are present in all of the identified top analogs; the top two compounds, 4G and 7D, contain both of these fragments.
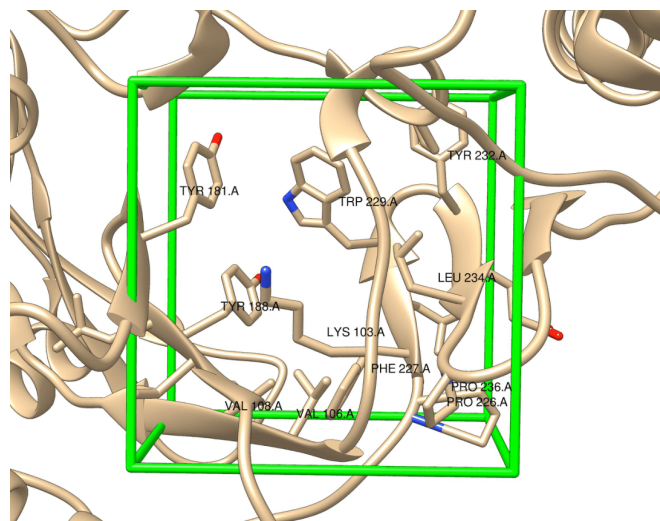

Figure 5: Computational parameters. Reverse transcriptase (PDB: 3MEE) with the docking parameters, a 16 by 16 by 16 Å box centered at the center atom of rilpivirine (9.200, 13.002, 20.250) visualized in green.

We hypothesize that the halogen in the trifluoromethyl group and the hydrophobic interactions caused by the toluene group account for their success. Further computational studies will focus on the nitrile group present in rilpivirine, which can be reproduced through usage of various benzonitriles. Efforts towards the chemical synthesis and *in vitro* evaluation of hit compounds from this screen on HIV-RT are additionally currently underway. Physical synthesis and biological assays will then test the efficacy of the analogs computationally predicted to have biological activity.

METHODS
Modeling, Design, and Molecular Mechanics Preoptimization
The library of rilpivirine analogs was systematically created and modeled using Avogadro (24), an open-source molecular modeling software package, through 2,4 substitution of a 2,4-dichlorinated pyrimidine with a selection of 14 anilines, whose structures are listed and pictured in **Figure 4**. These substitutions then allowed for the design of 196 analogs. All chemical entities screened in this study were initially optimized by molecular mechanics using the UFF94 force field at 10,000 steps.

Density Functional Theory (DFT)
Input files for rigorous quantum-mechanical optimization were created through Avogadro. The geometries of each structure were thermodynamically minimized via density functional theory (DFT) through ORCA (25), an *ab initio* quantum molecular modeling software, using a B3LYP functional and def2-SVP basis set with a continuum solvation model (CPCM) in water. All DFT calculations were performed on a Dell PowerEdge 710 server with a 24 core Intel Xeon X5660 processor at 2.80 GHz and 32 GB RAM.

Molecular Docking
With a batch script (26) submission to AutoDock Vina (27), optimized structures were docked to the allosteric binding pocket of RT to predict binding affinities of our designed analogs. The unliganded structure of rilpivirine bound to a representative reverse transcriptase of HIV [PDB:3MEE (20)] was used as the receptors and internal standard for comparison. The center atom of rilpivirine (9.200, 13.002, 20.250) was set as the center of a 16 by 16 by 16 Å grid box (**Figure 5**). Predicted binding modes were preliminarily judged through the value of free energy of binding (ΔG) in kcal/mol. The final binding poses were visualized through Chimera (21) before the final docking positions and protein-ligand interactions were analyzed to extract both predicted binding thermodynamics and the structural basis for such results (**Figure 3**).

REFERENCES

1. "The Global HIV/AIDS Epidemic." *HIV.gov*, 7 July 2020, www.hiv.gov/hiv-basics/overview/data-and-trends/global-statistics.
2. "What Are HIV and AIDS?" *HIV.gov*, 18 June 2020, www.hiv.gov/hiv-basics/overview/about-hiv-and-aids/what-are-hiv-and-aids.
3. "HIV Treatment: The Basics." (n.d.). 7 January 2021, https://hivinfo.nih.gov/understanding-hiv/fact-sheets/hiv-treatment-basics
4. Sharp, Paul M., and Beatrice H. Hahn. "The evolution of HIV-1 and the origin of AIDS." *Philosophical transactions of the Royal Society of London. Series B, Biological sciences*, vol. 365, no. 1552, 2010, pp. 2487-94. doi:10.1098/rstb.2010.0031
5. Usach, Iris *et al.* "Non-nucleoside reverse transcriptase inhibitors: a review on pharmacokinetics, pharmacodynamics, safety and tolerability." *Journal of the International AIDS Society*, vol. 16, no. 1, 4 Sep. 2013, pp 1-14. doi:10.7448/IAS.16.1.18567
6. Behja, W., and M. Jemal. "Anti-HIV Drug Discovery, Development and Synthesis of Delavirdine: Review Article". *International Research Journal of Pure and Applied Chemistry*, vol. 20, no. 3, 2019, pp. 1-16. doi:10.9734/irjpac/2019/v20i330137.
7. Mbuagbaw, Lawrence *et al.* "Efavirenz or nevirapine in three-drug combination therapy with two nucleoside or nucleotide-reverse transcriptase inhibitors for initial treatment of HIV infection in antiretroviral-naïve individuals." *The Cochrane database of systematic reviews*, vol. 12, no. 12, 2016, doi:10.1002/14651858.CD004246.pub4
8. Azijn, Hilde *et al.* "TMC278, a next-generation nonnucleoside reverse transcriptase inhibitor (NNRTI), active against wild-type and NNRTI-resistant HIV-1." *Antimicrobial agents and chemotherapy*, vol. 54, no. 2, 2010, pp. 718-27. doi:10.1128/AAC.00986-09
9. Buscher, A *et al.* "Impact of antiretroviral dosing frequency and pill burden on adherence among newly diagnosed, antiretroviral-naive HIV patients." *International journal of STD & AIDS* vol. 23, no. 5, 2012, pp. 351-5. doi:10.1258/ijsa.2011.011292
10. Minuto, Joshua J, and Richard Haubrich. "Etravirine: a second-generation NNRTI for treatment-experienced adults with resistant HIV-1 infection." *Future HIV therapy*, vol. 2, no. 6, 2008, pp. 525-537. doi:10.2217/17469600.2.6.525
11. Ludovici, D W *et al.* "Evolution of anti-HIV drug candidates. Part 1: From alpha-anilinophenylacetamide (alpha-APA) to imidoyl thiourea (ITU)." *Bioorganic & medicinal chemistry letters*, vol. 11, no. 17, 2001, pp. 2225-8. doi:10.1016/s0960-894x(01)00410-3
12. Hwang, Carey *et al.* "Rational Design of Doravirine: From Bench to Patients." *ACS infectious diseases*, vol. 6, no. 1, 2020, pp. 64-73. doi:10.1021/acsinfecdis.9b00178
13. Wang, Yali *et al.* "Current and emerging non-nucleoside reverse transcriptase inhibitors (NNRTIs) for HIV-1 treatment." *Expert opinion on drug metabolism & toxicology*, vol. 15, no. 10, 2019, pp. 813-829. doi:10.1080/17425255.2019.1673367
14. Kang, Dongwei *et al.* "Structure-Based Bioisosterism Yields HIV-1 NNRTIs with Improved Drug-Resistance Profiles and Favorable Pharmacokinetic Properties." *Journal of medicinal chemistry*, vol. 63, no. 9, 2020, pp. 4837-4848. doi:10.1021/acs.jmedchem.0c00117
15. Kang, D., Zhao, T., Wang, Z. *et al.* "Discovery of piperidine-substituted thiazolo[5,4-*d*]pyrimidine derivatives as potent and orally bioavailable HIV-1 non-nucleoside reverse transcriptase inhibitors." *Commun Chem*, vol. 2, no. 74, 2019, https://doi.org/10.1038/s42004-019-0174-8
16. Janssen, P. J. *et al.* "In search of a novel anti-HIV drug: multidisciplinary coordination in the discovery of 4-[[4-[[4-[(1E)-2-cyanoethenyl]-2,6-dimethylphenyl]amino]-2-pyrimidinyl]amino]benzonitrile (R278474, rilpivirine)." *Journal of medicinal chemistry*, vol. 48, no. 6, 2005, pp 1901-9. doi:10.1021/jm040840e
17. Chen, Xuwang *et al.* "Recent advances in DAPYs and related analogues as HIV-1 NNRTIs." *Current medicinal chemistry*, vol. 18, no. 3, 2011, pp. 359-76. doi:10.2174/092986711794839142
18. Goebel, Frank *et al.* "Short-term antiviral activity of TMC278--a novel NNRTI--in treatment-naive HIV-1-infected subjects." *AIDS (London, England)*, vol. 20, no. 13, 2006, pp. 1721-6. doi:10.1097/01.aids.0000242818.65215.bd
19. Smith, Steven J *et al.* "Rilpivirine analogs potently inhibit drug-resistant HIV-1 mutants." *Retrovirology*, vol. 13, no. 11, 2016, doi:10.1186/s12977-016-0244-2
20. Lansdon, Eric B *et al.* "Crystal structures of HIV-1 reverse transcriptase with etravirine (TMC125) and rilpivirine (TMC278): implications for drug design." *Journal of medicinal chemistry*, vol. 53, no. 10, 2010, pp. 4295-9. doi:10.1021/jm1002233
21. Pettersen, Eric F *et al.* "UCSF Chimera--a visualization system for exploratory research and analysis." *Journal of computational chemistry*, vol. 25, no. 13, 2004, pp. 1605-12. doi:10.1002/jcc.20084
22. Anjana, Ramnath *et al.* "Aromatic-aromatic interactions in structures of proteins and protein-DNA complexes: a study based on orientation and distance." *Bioinformation*, vol. 8, no. 24, 2012, pp. 1220-4. doi:10.6026/97320630081220
23. Wensing, Annemarie M *et al.* "2019 update of the drug resistance mutations in HIV-1." *Topics in antiviral medicine*, vol. 27, no. 3, 2019, pp 111-121.
24. Hanwell, Marcus D., *et al. Journal of Cheminformatics*, vol. 4, no. 17, 2012, doi:10.1186/1758-2946-4-17.
25. Neese, Frank. "The ORCA Program System." *WIREs Computational Molecular Science*, vol. 2, no. 1, 2011, pp. 73–78. doi:10.1002/wcms.81.
26. Ashok, Bhavesh. "Bhaveshashok/AutoDockVina-BatchSubmission." *GitHub*, 2020, github.com/bhaveshashok/AutoDockVina-BatchSubmission.
27. Trott, Oleg, and Arthur J Olson. "AutoDock Vina: improving the speed and accuracy of docking with a new scoring function, efficient optimization, and multithreading." *Journal of computational chemistry*, vol. 31, no. 2, 2010, pp. 455-61. doi:10.1002/jcc.21334